energy&fuels

Article

pubs.acs.org/EF

In Situ Observation of Mesophase Formation and Coalescence in Catalytic Hydroconversion of Vacuum Residue Using a Stirred Hot-Stage Reactor

S. Reza Bagheri,[†] Murray R. Gray,[†] John M. Shaw,[†] and William C. McCaffrey[†,*]

[†]Department of Chemical and Materials Engineering, University of Alberta, Edmonton, AB Canada T6G 2V4

ABSTRACT: A microreactor equipped with a view window and a stirrer was used to observe mesophase formation in Athabasca vacuum residue with and without catalyst. The effect of stirring on mesophase formation and its growth and coalescence was studied during the cracking of vacuum residue under hydrogen at 4.8 MPa and 440 °C. Stirring can result in a bimodal distribution of size of mesophase domains. The forced coalescence of mesophase droplets by the stirrer led to the formation of very large mesophase regions (bulk mesophase), which coexisted with a large number of small micrometer-sized mesophase domains. The addition of catalyst likely had both chemical and physical effects on the formation and growth of mesophase. The catalyst gave a delay in the onset of mesophase formation as a chemical effect and a decrease in the amount of bulk mesophase regions by suppressing the coalescence of smaller mesophase domains as a physical effect. The analysis of the resulting cokes by scanning electron microscopy (SEM) showed that catalyst particles agglomerated and stuck to the outer surface of the mesophase domains and suppressed their coalescence. The agglomeration of catalyst particles likely decreased their ability to suppress the formation of small mesophase domains, in the range of a few micrometers in size. However, catalyst was effective in suppressing the formation of bulk mesophase domains with areas over 2000 μm^2. The results showed that the onset of observable mesophase initially increased with the addition of catalyst, but then decreased at higher catalyst concentrations. SEM observation confirmed that the significant agglomeration of catalyst particles at higher concentrations was likely responsible for the decreased effectiveness of the catalyst in suppressing mesophase formation.

INTRODUCTION

The use of hydrogen in catalytic processes was one of most important advances in refining technology during the twentieth century.[1] This process uses the fact that the presence of hydrogen during a thermal reaction of petroleum feedstocks prevents many of coke-forming reactions and improves the yields of the lower boiling components such as gasoline, kerosene, and jet fuel.[2] The cracking and hydrogenation of heavy hydrocarbon molecules and the removal of heteroatoms result in a product with lighter oil fractions and a lower level of contaminants with an increased commercial value and less pollution.[3] The formation of coke during the upgrading of heavy oil is an area of significant importance because of its effect on reducing the liquid yield, catalyst deactivation, and fouling of reactor internals and downstream vessels.[4] Coke is usually defined in the petroleum industry as toluene insoluble material,[4] and coke formation is triggered by reactions such as cracking, polymerization, and condensation, which results in the formation of coke as a new carbonaceous phase. Phase behavior also plays an important role in the formation of coke.[5]

Carbonaceous mesophase is an intermediate phase that can form during the cracking of heavy oil, as a subset of toluene-insoluble or coke phases, which is distinguished by its optical anisotropy.[6] During the thermal cracking of heavy petroleum and coal tar fractions, Brooks and Taylor[7] observed the formation of an intermediate condensed phase, which is anisotropic when viewed under polarized light. This carbonaceous mesophase is now classified as a discotic nematic liquid crystal.[8] Carbonaceous mesophase appears during the thermal conversion of heavy oil, in the temperature range between 350 and 500 °C, as optically anisotropic spheres surrounded by an isotropic liquid matrix. Cracking of heavy oil gives formation of polycondensed aromatic hydrocarbons, by polymerization, cyclization, dealkylation, and dehydrogenation reactions. The mesophase spherules form as a result of the accumulation of layers of oriented polycondensed aromatic hydrocarbons.[9] Important factors in the mesophase formation process are the heating rate, temperature, residence time, gas flow rate, and stirring rate.[9] Once mesophase spheres begin to form, they can coalesce to form larger mesophase domains. These larger domains eventually deposit as coke on the interior surfaces of process equipment. If the coalescence process can be hindered or ideally prevented, the size of mesophase domains would be smaller and, consequently, be carried out of the process lines and vessels without fouling the equipment.[10]

The slurry hydroconversion processes utilize finely dispersed catalysts, which can be introduced into the feed as water-soluble or oil-soluble precursors or as finely divided powders.[11] Several slurry hydroconversion demonstration plants have been built so far, including the CANMET process at the Petro-Canada Montreal Refinery (constructed in the mid-1980s).[12] Currently, these technologies are still at the demonstration scale. Typically, in the hydroconversion of heavy oils, the main reaction is thermal cracking that produces lower boiling point products. The role of catalyst and hydrogen is to inhibit coke formation by hydrogenating reactive products such as olefins

Received: February 24, 2012
Revised: May 10, 2012
Published: May 15, 2012

   dx.doi.org/10.1021/ef300321g | *Energy Fuels* 2012, 26, 3167–3178

and removing heteroatoms.[13,14] Kennepohl and Sanford[15] and Panariti et al.[16] showed that dispersed catalysts such as molybdenum sulfide or molybdenite have the ability to prevent coke formation at low catalyst concentrations. At higher concentrations, however, catalysts can promote coke formation. In addition to a chemical role, the catalyst particles act as supporters or nucleation sites for coke and, hence, reduces coking of the reactor walls.[17]

The formation of mesophase can be studied by various methods, but polarized-light microscopy is generally the most useful method, because carbonaceous mesophase was discovered and defined by its optical anisotropy.[7] In hot-stage microscopy, a heated microreactor is placed on the optical stage of a polarized light optical microscope to enable the in situ observation mesophase growth at the conditions of formation.[18] The first in situ observations of mesophase formation was done by Lewis[19] in 1975 using a modified hot-stage apparatus with a glass cover. Perrotta et al.[20] observed the in situ mesophase formation in petroleum and coal tar pitch at elevated temperatures and pressures. They used a custom reactor for high pressure observations. Rodriguez et al.[21] also designed a high pressure and high temperature hot-stage to observe the in situ mesophase formation in petroleum fractions. Lafdi et al.[22] used hot-stage microscopy to study anisotropic pitches, and Rahimi et al.[23] studied the incipient mesophase formation of 10 fractions from Athabasca bitumen vacuum bottoms using hot-stage microscopy under flowing hydrogen at 5.2 MPa. All these studies used an upright reflective microscope, and samples in the hot-stage were not subjected to stirring. Lewis[19] used a metal probe inserted into the hot-stage chamber to agitate the sample, but not an effective stirrer or agitator. All other studies on pressurized samples were conducted without agitation.

The interpretation of kinetic data from laboratory and pilot scale slurry hydroconversion processes is complicated due to the lack of a physical understanding of the reaction progress. Hot-stage microscopy can be used to gain further insight into the chemistry and physics of the reacting system at process conditions. The results obtained by hot-stage microscopy, however, can not be easily up-scaled to real reactors. It is important to note that the purpose of this study is not to produce kinetic data to be used in reactor design. Our goal is to gain a physical insight of the slurry conversion process using hot-stage microscopy that we hope will be useful in understanding the processes happening inside industrial reactors. Based on the results obtained with a hot-stage microreactor, we can build models and suggest mechanisms that are testable in laboratory, pilot, or industrial scale reactors.

The amounts of mesophase in a sample can be determined quantitatively by room temperature polarized microscopy. Using such a technique, Chwastiak et al.[24] developed a quantitative method for measuring the amount of mesophase in reaction products. They collected micrographs of six randomly selected areas of mounted and polished sample, calculated the area fraction of mesophase in these micrographs by image processing, and averaged the results. They demonstrated that the results were repeatable and statistically valid for measuring the mesophase content of the mesophase pitch at solidification. Lewis et al. developed quantitative procedures for measuring the average size of mesophase domains. Moriyama et al.[25] also used polarized microscopy for quantitative analysis of mesophase formation and for determination of the population density and size distribution of the mesophase spheres. They collected images of the polished surface of the sample and calculated the average population density. The results showed that increasing the number of images could reduce the statistical deviations; however, they showed that the minimum number of 7 images was sufficient for reproducibility of the population density.

The effect of catalyst on mesophase formation has been studied previously. Braun et al.[26] studied iron-catalyzed pyrolysis of coal-tar pitch using iron benzoate and naphthoate as catalyst precursors. They showed that, with iron benzoate, the nucleation and growth of mesophase spheres are strongly influenced by the catalyst, with a reduced tendency for coalescence to form large mesophase domains. Bernhauer et al.[27] reported similar results when ferrocene was used as a catalyst precursor. However, these results were based on the examination of cooled products, not in situ observations. In situ study of mesophase formation during catalytic hydroconversion using hot-stage microscopy has not been previously reported, mainly due to the inability of the previous designs to stir the fluid under observation in a hot-stage microscope.

In this paper we report for the first time the use of a stirred hot-stage reactor to observe the effect of stirring on mesophase formation and growth in Athabasca vacuum residue. The experiments were conducted with and without stirring to be able to compare the results. The use of a stirred hot-stage apparatus allowed us to suspend heterogeneous catalyst in the reacting liquid and study the effect of catalyst on mesophase formation and growth. The resulting cokes were observed with scanning electron microscopy (SEM) to reveal the possible interactions between mesophase and catalyst particles.

EXPERIMENTAL SECTION

Materials. Athabasca vacuum residue supplied by Syncrude Canada was used for observations, and its properties are shown in Table 1. The catalyst was a proprietary nanoparticulate material consisting of transition metal sulfides.

Table 1. Properties of Athabasca Vacuum Residue

elemental analysis	C (wt %)	81.76
	H (wt %)	9.45
	S (wt %)	6.17
	N (wt %)	0.93
asphaltene (wt %)		31.1
MCR (wt %)		14.9
ash (wt %)		3.3
solids (wt %)		0.22

Characterization of Catalyst. Brunauer–Emmett–Teller (BET) surface area of catalyst was determined from N_2 adsorption–desorption isotherms measured at 77 K using a Micromeritics ASAP 2020 analyzer. Sample was degassed in 523 K under vacuum (500 μm) for 8 h before being analyzed. Eight N_2 uptake measurements made in the range $0.06 < P_{N_2}/P0_{N_2} < 0.2$ were used to calculate the BET surface area.

Hot-Stage Microscopy. Reactions were carried out in a new hot-stage reactor, which has been discussed in detail elsewhere.[28] A schematic design of the hot-stage is shown in Figure 1. The hot-stage reactor was configured to interface with an inverted reflective microscope. The reaction chamber was made of stainless steel Swagelok fittings with a sapphire window at the bottom to facilitate the observation of the sample inside it. The temperature of the hot-stage is maintained by a heating tape connected to a temperature controller, and it is thermally insulated by ceramic covers. Reaction temperature is monitored by an Omegaclad XL type K $^1/_{16}$″

dx.doi.org/10.1021/ef300321g | Energy Fuels 2012, 26, 3167–3178

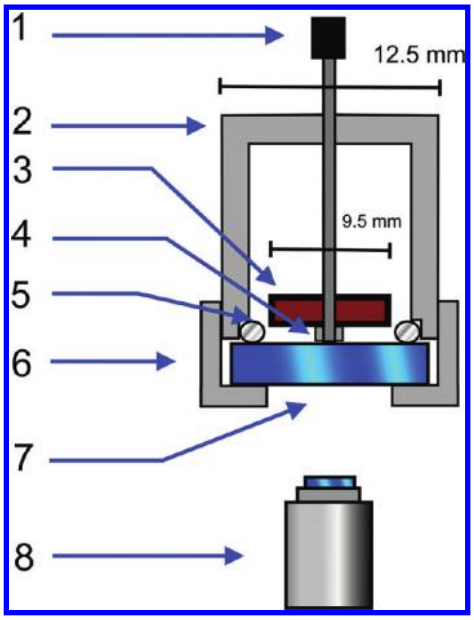

Figure 1. Schematic diagram of the hot-stage reactor: 1, thermocouple; 2, steel body; 3, magnet; 4, metal washer; 5, O-ring; 6, bottom nut; 7, sapphire windows; 8, objective lens of microscope.

thermocouple inserted into the top of the hot-stage, which is in direct contact with the sapphire window. The tip of the thermocouple acts as shaft for the magnet stirrer (Figure 1). A custom built Alnico magnet stirrer was used in this hot-stage reactor to mix the reactor contents. The stirrer is a block magnet (9.5 × 4 × 3 mm) with a 2 mm hole at the center for the thermocouple. The stirrer is coupled with an external magnet rotating at 140 rpm. A stainless steel washer (thickness 0.13 mm, diameter 2.7 mm, provided by Boker's Inc., Minniapolis) is used to raise the magnet from the window (Figure 1).

A mass of 0.4 g of each sample was heated in the reactor to 440 °C under continuous stirring at 140 rpm (For the nonstirred experiment the initial mass was 0.25 g). Experiments were conducted under a hydrogen atmosphere that was maintained at 4.8 MPa. The onset of mesophase formation was determined for all the samples by using a Zeiss Axio-Observer inverted reflective microscope (Zeiss, Germany) equipped with crossed polarizers. A Zeiss 3 megapixel camera was connected to the microscope to photographically record the progress of the reaction. Image analysis was performed on a personal computer using ImageJ, a program developed at National Institutes of Health (U.S.A.). The images were analyzed to determine the area fraction of observable mesophase particles and their mean area in each photo. In the image analysis, particles with areas smaller than 3 μm^2 were excluded from the results because such small domains could not be accurately identified.

To follow the progress of the nonstirred experiment, one random spot was chosen, and the formation and growth of mesophase at this spot was followed by taking images at different times. For the experiments with the stirred-reactor, the experimental procedure for taking the photos was as follows: before taking the photos, the stirrer was turned off for 4 min to give enough time for sedimentation; after sedimentation, seven photos were taken at random locations, showing the mesophase visible on the window; stirring was turned on again, and the same procedure was repeated. The time of reaction shown for all the graphs in this paper begins when the reactor is heated to the set-point temperature, and the reported time for each set of data was the average of the times at which all seven photos were taken. Acquiring seven photos under in situ conditions took approximately 3 min. The total area covered by the seven photos was 6.34 mm^2. The photos were analyzed using ImageJ, and the results of the all images combined to determine the observable mesophase area fraction in the hot-stage at each time. Ideally, an estimate of the volume fraction of mesophase would be used to follow the progress of the reactions. Calculating the mesophase volume from images was not practical, however, due to the limitations of the hot-stage microscope technique, and therefore, the data is reported as area coverage of the viewable area (μm^2). Due to the presence of a bimodal distribution of mesophase particles, the image analysis was done separately for the first and second modes of the distribution (the second mode generally began for particles with areas above 2000 μm^2).

SEM and EDX. Samples were observed using a high resolution JEOL 6301F field emission scanning electron microscope. Energy-dispersive X-ray (EDX) analysis was done via a PGT X-ray analysis apparatus (res. 135 eV). In addition, some samples were freeze-fractured in liquid nitrogen and the cross-section was observed by SEM. Samples were sputter-coated with carbon before the observation.

RESULTS AND DISCUSSION

Cracking of Vacuum Residue under Hydrogen in Absence of Stirrer. A mass of 0.25 g of Athabasca vacuum residue was cracked under hydrogen at 4.8 MPa and 440 °C without catalyst. In this set of experiments, it was important that hydrogen should diffuse into the bitumen film and reach the interface between bitumen film and sapphire window. Therefore, it was important that the sample should be thin enough to provide the required concentration of hydrogen throughout the liquid layer. Fortunately, at the reaction conditions used in this study, the cracking and hydrogenation reactions are relatively slow, with residence times on the order of 1 h or more,[11] and the solubility of hydrogen is significant on a molar basis.[29] Using these data and an estimated diffusion coefficient of 1.13×10^{-8} m^2/s, we calculated that a liquid film thickness of up to 1.7 mm would ensure that the dissolved hydrogen concentration was at least 80% of saturation. This thickness corresponded to a sample mass of 0.25 g in our reactor. The reacting fluid in the nonstirred sample could have an average temperature that is higher than the set-point temperature. The thermocouple is placed in the center of the sapphire window (Figure 1), which is the coldest part of the sample because of the thermal convection from the window. As a result, the fluid closer to the wall of the reactor would be hotter than the temperature shown by the thermocouple. With this provision, mesophase was first observed 27 min after reaching the nominal set-point temperature of 440 °C. The initial domains were very small, and the areas of the biggest domains were around 5 μm^2. In this unmixed mixture, mesophase did not form uniformly in the field of view through the window, and at some spots, mesophase was not observed at all during the experiment. Figure 2 shows the mesophase area fraction of this reacting mixture versus time of reaction. The time course follows a sigmoid-shape curve, which is commonly observed in phase transformations such as solidification and crystallization.[30] The sigmoid-shape curve is consistent with a nucleation growth process, in which the new phase forms by random nucleation in the bulk of the fluid or continuous phase, and then, these nuclei grow.[30] The growth occurs at the interface between the old and new phases. As the reaction proceeds, the interface increased constantly, giving an acceleration of rate of formation of mesophase up to an inflection point. Given the low area fraction of mesophase in the micrographs, two reasons are likely responsible for the reduction in rate at long reaction times: depletion of the mesophase precursors in the liquid (the micro-carbon residue (MCR) of the sample is 14.9%, which means there is a finite amount of coke that can be made during thermal reactions) or increased viscosity in the liquid due to the progressive thermal alteration of the feed (the bulk liquid viscosity will decrease, but

dx.doi.org/10.1021/ef300321g | Energy Fuels 2012, 26, 3167−3178

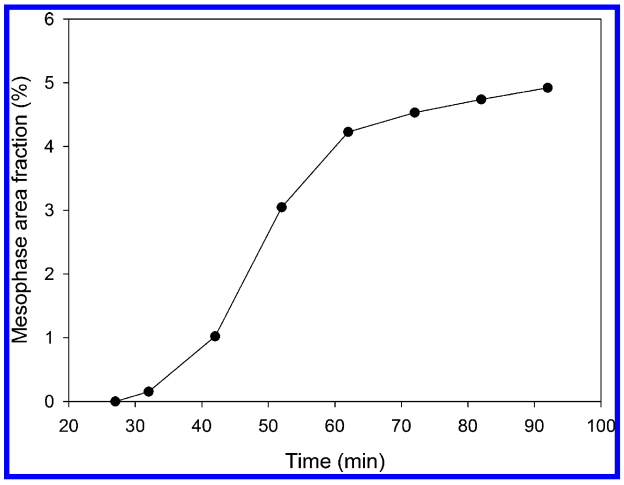

Figure 2. Mesophase area fraction versus time during the cracking of Athabasca vacuum residue under hydrogen at 4.8 MPa and 440 °C without stirring. Zero time was defined as the point when the reactor was heated to the final temperature. Data points are shown only when detectable mesophase was observed. Prior to the onset time no mesophase was detected, and no data points are shown.

the viscosity of mesophase will increase with time). Figure 3 shows the particle area distribution in this mixture 92 min after

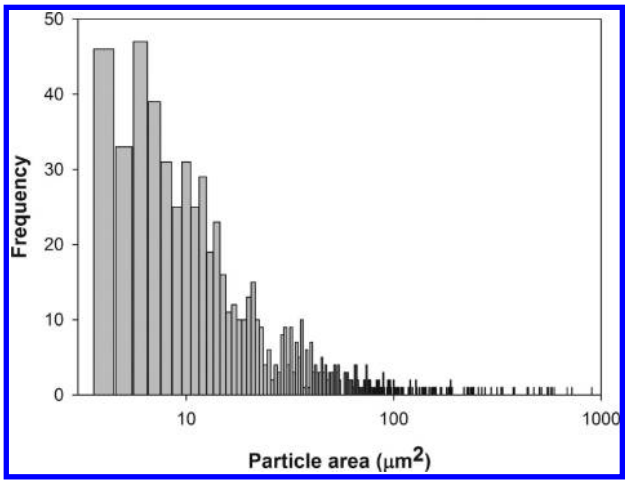

Figure 3. Particle area distribution for mesophase particles after 92 min during cracking of Athabasca vacuum residue under hydrogen without stirring at 4.8 MPa and 440 °C.

reaching the set-point temperature. An important feature that should be noted is the monomodal nature of the particle area distribution. This type of distribution was only observed in the absence of mixing.

Cracking of Vacuum Residue under Hydrogen with Stirring. A sample of Athabasca vacuum residue was cracked under hydrogen at 4.8 MPa without catalyst. The stirrer was turned on when the temperature reached 300 °C. Unfortunately, mesophase particles can not be observed while the hot-stage reactor is being stirred. Therefore, after reaching the final temperature, the stirrer was turned off every 2 min to check for the onset of mesophase formation. Mesophase was first observed in this experiment at 45 min after reaching the set-point temperature (the average time was 46.0 ± 1.7 min for 3 runs). With mixing, the temperature of the reacting fluid should be much more uniform and closer to the set-point, 440 °C, than in the case of the unmixed reactor. Since the kinetics of mesophase formation is known to be sensitive to temperature, the on-set times for the mixed and unmixed reactions should not be compared.

Notably, the distributions of mesophase domain sizes are different between the stirred and unstirred cases. As mentioned previously, a monomodal size distribution was observed in the unmixed case. To make sure that the result was not dependent to the mass of the sample, the unmixed experiment was repeated with 0.4 g of sample, but the size distribution remained monomodal. When the reactor contents were mixed, a bimodal distribution of mesophase domains was observed. The initial mesophase observed when the reactor was agitated was characterized by a few large domains formed in the bulk, and the areas of the largest domains were around 4500 μm^2, as shown in Figure 4. At the same time, a few smaller domains

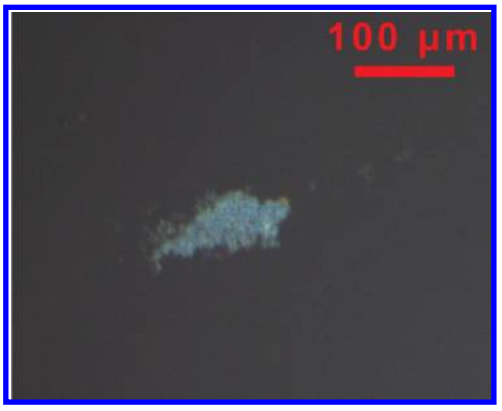

Figure 4. Photomicrograph of initial mesophase observed during cracking Athabasca bitumen under hydrogen at 4.8 MPa and 440 °C with agitation at 140 rpm as an aggregated domain.

(4−60 μm^2) were also observed, but the total area fraction of these smaller domains (0.01%) was much smaller than that of the large domains (0.2%). The large regions were probably the result of the coalescence of smaller mesophase domains, and we call this material "bulk mesophase". Bulk mesophase is usually defined as a continuous anisotropic phase formed by coalescence of mesophase spheres.[31] This definition of bulk mesophase is qualitative, however, and in this paper, we define bulk mesophase as any domains in the larger mode of the bimodal distribution (generally bigger than 2000 μm^2). With this operational definition, the majority of the domains observed at the onset of mesophase formation were characterized as bulk mesophase. This observation was completely different from what observed in the nonstirred reactor, in which all the initial detectable domains were smaller than 2 μm^2. In the mixed case, smaller mesophase domains were observed 8 min after the observance of large bulk domains, and these domains grew with time. Consequently, the reactor contained both mesophase spheres (small domain) and bulk mesophase (large domain) at the same time, as shown in Figure 5. Both the large domains and the small domains were mobile, in that they were suspended in the fluid phase and were easily moved by the action of the stirrer.

As noted, mixing of the reacting fluid resulted in the formation of a bimodal distribution of mesophase in the reactor. To show this bimodal distribution, the particles were divided into two groups: the first mode of the distribution was comprised of particles with area below 2000 μm^2, which formed

dx.doi.org/10.1021/ef300321g | Energy Fuels 2012, 26, 3167−3178

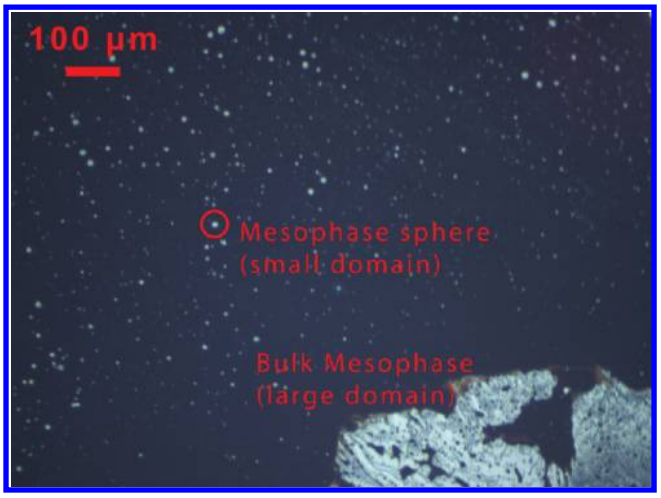

Figure 5. Photomicrograph of mesophase formed during cracking Athabasca vacuum residue under hydrogen at 4.8 MPa and 440 °C stirred at 140 rpm, showing coexistence of mesophase spheres (small domain) and bulk mesophase (large domain) formed by stirring after 85 min.

the small mesophase domains, and the second mode of the distribution included particles with area above 2000 μm^2, which formed the large mesophase domains (bulk mesophase). The total number of mesophase particles per unit area in the field of view was calculated at different times for both groups and is shown in Table 2; the area fraction of both groups is shown in Figure 6. Each of the data points is calculated from seven images that were taken over a period of 3 min, during which time the reactions were proceeding. The results of Figure 6 show that the total mesophase area fraction increased 1.7% over approximately the 3 min time span. This change limits the number of photos that can be used to calculate each data point. The area fraction of bulk mesophase regions (area above 2000 μm^2) was much larger, but it was from a much smaller number of particles. In spite of their limited number, the size of the bulk mesophase domains grew rapidly, and they soon became too big to fit into the field of view of the microscope; thus, it is possible that the total area of these regions was much greater than the reported value. These large domains were not observed in the absence of the mixing, so it is likely that these domains were the result of the forced coalescence caused by mixing. Figure 7 shows a typical distribution of the particle area in the reaction mixture at different times. The distributions for particles below and above 2000 μm^2 were drawn separately because of the very different range of particle size and frequency in each group.

Table 2. Number of Mesophase Domains Per Area (mm^2) with and without the Addition of Catalyst[a]

no catalyst			with 1.0 wt % catalyst		
time (min)	no. small domains per area (mm^{-2})	no. large domains per area (mm^{-2})	time (min)	no. small domains per (mm^{-2})	no. large domains per area (mm^{-2})
45	3.15	0.47	55	4.10	0.00
53	1.46×10^2	0.16	71	5.05×10	0.47
69	9.00×10^2	0.95	87	5.28×10^2	1.73
85	8.39×10^2	3.78	103	1.02×10^3	3.31
101	9.69×10^2	3.63	119	1.62×10^3	2.84
117	5.03×10^2	8.67	135	1.97×10^3	1.73

[a]Small domains have an area below 2000 μm^2, and large domains have an area above 2000 μm^2.

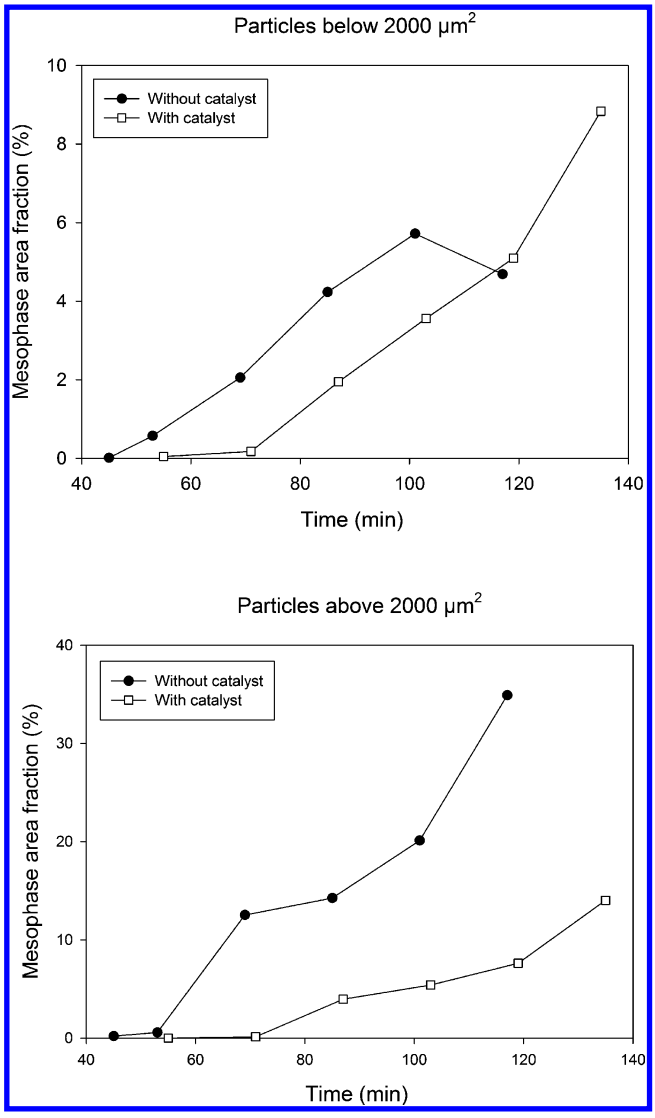

Figure 6. Mesophase area fraction during cracking of Athabasca vacuum residue under hydrogen at 4.8 MPa and 440 °C stirred at 140 rpm without catalyst and with 1.0 wt % catalyst for (a) small domains with area below 2000 μm^2 versus time, (b) large domains with area above 2000 μm^2 versus time of reaction. Data points are shown only when detectable mesophase was observed. Prior to the onset time, no mesophase was detected, and no data points are shown.

The data from the experiments with mixing clearly show a bimodal distribution of particle areas and implicitly show particle sizes. Given the mild agitation in the reactor and the fluid properties, turbulent eddies are unlikely to break up the mesophase domains, except perhaps the very largest over 2000 μm^2, which did not fit in the field of view of the microscope.[32] Mixing clearly alters the coalescence of the mesophase particles, giving a bimodal distribution, but how does this distribution arise, and why are the domains found at the onset of mesophase observation are so large?

Aggregative processes are known to produce bimodal distributions because aggregation introduces a second population of particles that are distinctly larger than the primary particles.[33] This type of aggregation has been observed in solid/liquid and gas/liquid systems. Shields et al. studied the thermal

dx.doi.org/10.1021/ef300321g | Energy Fuels 2012, 26, 3167−3178

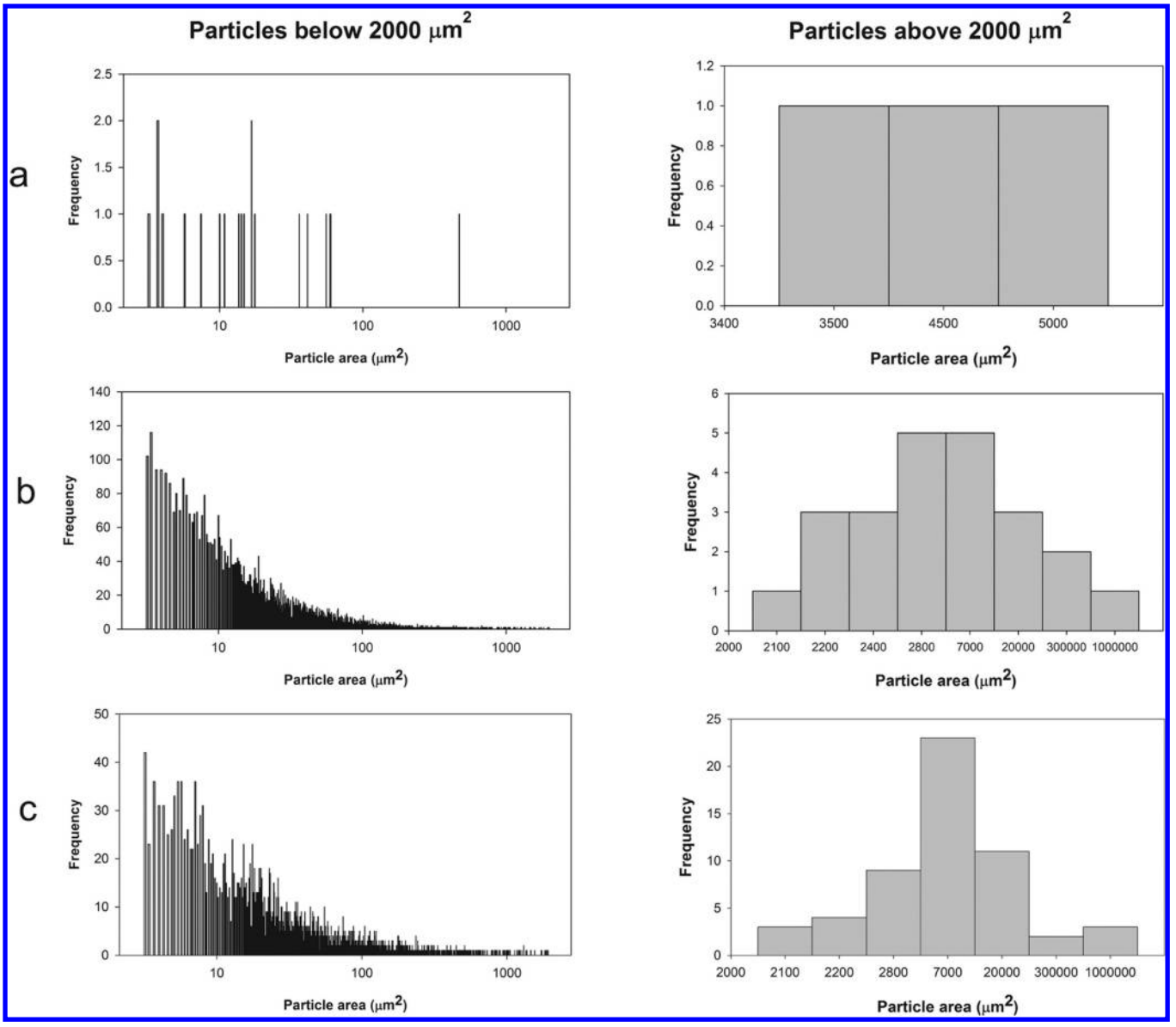

Figure 7. Particle area distribution for particles with area below and above 2000 μm^2 at different time of reaction in cracking of Athabasca vacuum residue under hydrogen at 4.8 MPa and 440 °C stirred at 140 rpm.

coarsening of decanethiolate-capped gold nanocrystals at various tetraoctylammonium bromide concentrations.[33] The coarsening kinetics were determined by measuring nanocrystal size distributions as a function of time. They reported the observation of bimodal nanocrystal size distribution at intermediate stages of coarsening.

The aggregation of solid lipid nanoparticles in a lipid/surfactant/water mixture leads to a bimodal distribution of aggregate size.[34] Monnoyer et al.[35] studied the formation of silver bromide particles, by mixing two microemulsions containing the precursors salts $AgNO_3$ and KBr. When the concentration of reactants was increased, it changed from an monomodal to a bimodal size distribution. A further increase of the concentration leads to a separation of the two mean sizes. Tojo et al.[36] used Monte Carlo simulation to study the influence of parameters like number of reagent molecules per droplet, surfactant film flexibility, droplet size, and presence or absence of autocatalysis by the product in formation of nanoparticles in microemulsions. They found that autocatalyzed reactions with high reagent concentrations and low surfactant film flexibility can result in a bimodal particle size distribution. To check further appearance of bimodality at high concentrations, we have prepared Pt particles in water/Brij30/*n*-heptane microemulsions using different precursor concentrations. The results clearly showed the appearance of bimodality at high concentration. Park et al.[37] did a numerical study of aerosol dynamics to obtain axially and radially varying size distributions of particles generated during the modified chemical vapor deposition process. The results predicted the bimodal size distributions both in flow and in the deposited layer, which were caused by the combination of particle generation and coagulation. The size distribution of particles will become bimodal because of the nucleation of small size particles and growth of generated particles due to coagulation.

The formation of rain drops is another example of a bimodal distribution. Rain droplet growth is initially dominated by condensation which results in a narrow distribution of small particles. The formation of larger drops is the result of collision

dx.doi.org/10.1021/ef300321g | *Energy Fuels* 2012, 26, 3167−3178

and subsequent coalescence, which is called "collection".[38] While initial rain droplet growth is dominated by condensation in the earliest stages of cloud development, subsequent growth is dominated by collisions and coalescence of the fraction of larger droplets. A large droplet can absorb a very large number of smaller droplets. The result is an explosive growth, which results in a bimodal distribution of droplet size.[39] The computations of Berry and Reinhardt[40] showed that a monomodal narrow size distribution can change into bimodal distribution.

By analogy to these examples, we can suggest an explanation for our observations. When the mesophase domains form, they initially are submicrometer in size, and form a monomodal distribution that is below the resolution of an optical microscope (Figure 8). The mode of this distribution can

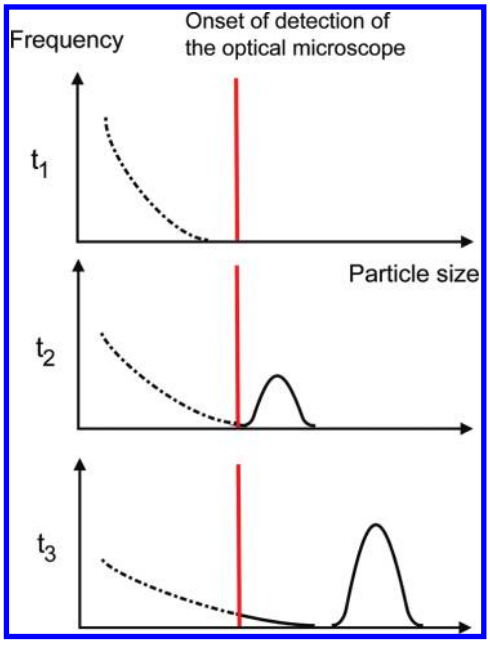

Figure 8. Time evolution of particle size distribution during mesophase formation in a stirred reactor (time: $t1 < t2 < t3$).

shift to larger particles with time, but most of it always remains at submicrometer-scale below the resolution of an optical microscope (Figure 8). When measured optically, the first mode has an asymptotic shape, which is consistent with other studies of particle growth by aggregative processes[33] (Figures 3 and 7). It is also possible that this mode was a truncated Gaussian distribution, but its peak was below the resolution of the microscope. Due to the limits of optical microscopy, the actual shape of the first mode cannot be determined. In absence of stirring, the distribution remained monomodal at all times (Figure 3). The addition of stirring can enhance the collision-coalescence process and change this initially monomodal distribution into a bimodal distribution (Figure 7). Therefore, two modes will be present in the system: the first mode due to the generation of submicrometer mesophase domains caused by chemical reactions and the second mode due to the coalescence of these domains. Apparently, when the second mode of larger mesophase particles initially forms, the first mode of the particle size distribution is just below the resolution of the optical microscope (with the exception of a few large domains) and is not observed (Figure 8). As a result, the initial domains, which were observed at the onset of mesophase formation, were composed of a few large domains (from the second mode) accompanied with a few small domains (from the first mode) (Figure 8). After formation, the number and size of domains in the second mode continually grows at the expense of diminishing first mode's domains (Figure 8).

To understand how stirring affects the observed size distribution, first we suggest, in Figure 9a, a series of reactions and physical changes that are responsible for the formation and growth of mesophase. The combination of thermal cracking, addition, and condensation reactions in the vacuum residue leads to the formation of high molecular weight planar polyaromatic molecules. These molecules can stack to give mesophase domains, which are initially too small to be detected by an optical microscope (Figure 9a). As conversion of vacuum residue proceeds, these mesophase domains can grow by the addition of molecular clusters resulting from addition reactions and condensation of more polyaromatic aromatic molecules (Figure 9b). The mesophase domains, when contacted with each other, can also coalesce instantaneously to form larger mesophase domains[41] (Figure 9c). The growth and coalesce of mesophase domains continue until they become observable with an optical microscope as micrometer-scale mesophase spheres. The further coalescence of these micrometer-scale mesophase spheres can result in the formation of bulk mesophase (Figure 9d). The combination of steps a, b, c, and d in Figure 9 would give rise to the initial monomodal distribution and results in the formation of a large number of submicrometer mesophase domains with or without mixing. Stirring forces the coalescence of the submicrometer domains with each other (Figure 9e excluding the micrometer-scale mesophase spheres on the left side) to form the second mode of size distribution for bulk mesophase. The formed bulk mesophase can also grow by collecting more submicrometer domains (Figure 9f). When the population of these large domain increases, however, they can coalesce both with each other and with smaller micrometer-scale mesophase spheres to form even larger domains (Figure 9g and h).

Cracking of Vacuum Residue under Hydrogen with the Stirrer and Catalyst. A sample of Athabasca vacuum residue was premixed with 1.0 wt % of catalyst and reacted under hydrogen at 4.8 MPa. The stirrer was turned on when temperature reached to 300 °C. After reaching the set-point temperature, the stirrer was turned off every 2 min to identify the onset time of mesophase formation. Mesophase formed 55 min after reaching the set-point temperature (the average time was 60.3 ± 6.1 min for 3 runs). As expected, the addition of catalyst gave a longer time to onset, in this case, 10 min longer than the experiments with only hydrogen and mixing. Similar to the experiments without catalyst, the first observed mesophase particles were the larger bulk type mesophase particles and they could be moved easily by the motion of the stirrer.

The initial mesophase observed when the reactor was agitated without catalyst and was dominated by a few large domains formed in the bulk, and the areas of the largest domains were around 4500 μm^2, as shown in Figure 4. In contrast, the initial mesophase domains observed in the presence of catalyst consisted of smaller domains of bulk mesophase, with areas of around 950 μm^2. Some smaller domains, as small as 3 μm^2, were also observed at the same time. Initially, the total area fraction of these smaller domains (0.006% for domains between 3 and 100 μm^2), however, was much smaller than that of the larger domains (0.044% for

dx.doi.org/10.1021/ef300321g | Energy Fuels 2012, 26, 3167−3178

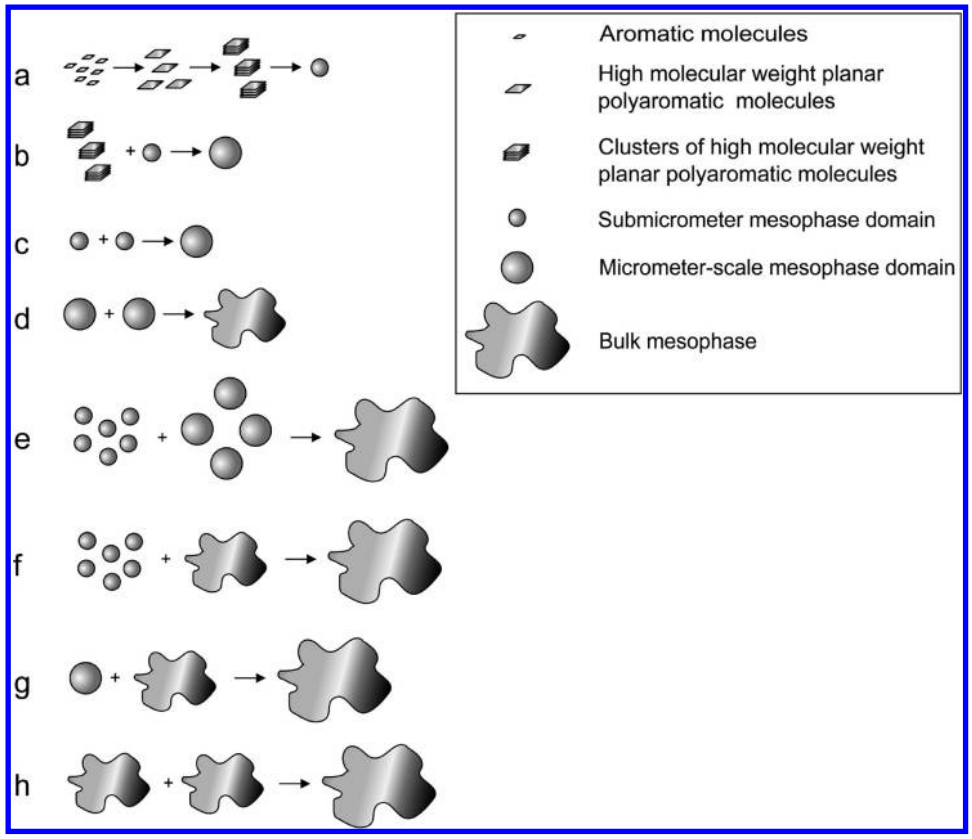

Figure 9. Different mechanisms for the formation and growth of mesophase.

domains larger than 100 μm^2). Note that with the addition of catalyst, the median size of second mode of the particle size distribution, or bulk mesophase, was smaller than in the case of the stirred uncatalyzed reactions. The majority of the initial domains were still much larger than in the case of the unmixed reaction. The spherical domains of mesophase were observed in large numbers 16 min after the onset of mesophase observation and grew with time, so at this time the reactor fluid contained significant amounts of both small mesophase spherules and bulk mesophase. As in the experiment without catalyst, the stirring resulted in the formation of a bimodal distribution of mesophase. The area fractions and total number of mesophase particles per unit area were calculated at different times for particles in both modes of the bimodal particle size distribution and are shown in Figure 6 and Table 2. The particle areas for particles in the first mode of the distribution again had an asymptotic shape, as in the previous experiment. Also as in the previous experiment, the area of the bulk mesophase domains grew rapidly to become and too large to fit into the field of view of the microscope.

The addition of catalyst increased the time for onset of mesophase formation as expected. The slope of the curves for the middle points in Figure 6a was very close, which indicated that the rates of growth for the small particles in the first mode of the distribution, below 2000 μm^2, were almost the same with and without catalyst. However, the addition of catalyst significantly suppressed the rate of formation of the large particles with area above 2000 μm^2, as shown in Figure 6b. The addition of catalyst apparently suppressed the driving forces for coalescence of spheres to form bulk mesophase, which resulted in a lower area fraction of bulk mesophase. This observation was also consistent with the previous study by Braun et al.[26] who showed that iron sulfide catalysts derived from ferrocene and especially iron benzoate could significantly reduce the coalescence of mesophase domains, giving a much longer time to form bulk mesophase. Their SEM analysis showed that catalyst particles were located at the surface of mesophase spheres; therefore, they suggested that the surface coverage of the spheres could be responsible for the hindrance of coalescence.[26,27]

In this study, the coke that remained in the reactor after the cracking of vacuum residue under hydrogen with stirring and catalyst was collected after finishing the experiment. Figure 10 shows the surface of this coke by SEM. The mesophase particles were easily detectable due to their higher density giving brighter domains, and the catalyst particles were also detectable as even brighter particles in the photo. This analysis was confirmed by EDX analysis of the sample (Figure 10a). The image showed that the catalyst only attached to the outer surface of mesophase and did not penetrate into mesophase domains as suggested by previous studies.[26,42] With the catalyst collected on the surface of the mesophase domains, there are two possible mechanisms by which the catalyst could reduce the formation of bulk mesophase: a chemical mechanism and a physical mechanism.

Chemically, it is well-known that the addition of hydrogen and an active hydrogenation catalyst can reduce the formation of coke during the thermal cracking of heavy oil. One possible role of the catalyst is to reduce the addition reactions that are thought to precede mesophase formation (Figure 9a). Gray and McCaffrey[43] suggested that the key role of the catalyst is preventing olefin addition reactions by promoting direct olefin conversion and partial hydrogenation of polynuclear aromatic hydrocarbons to form donor species. Polymerization of olefins

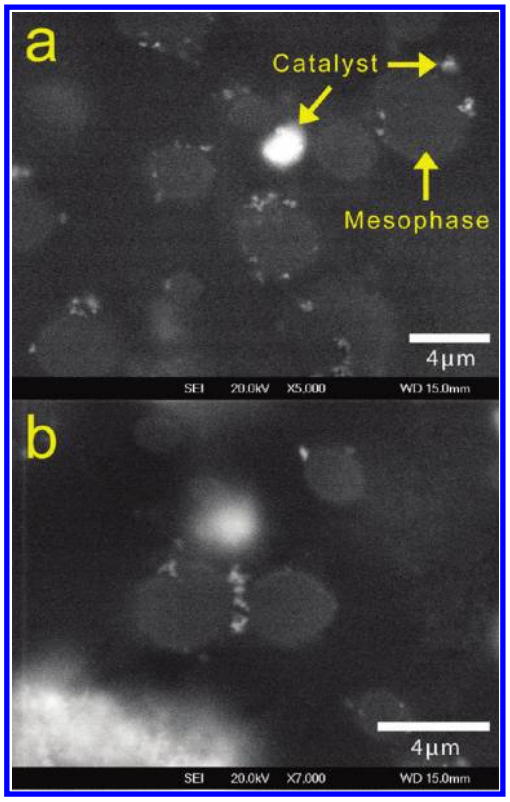

Figure 10. SEM photograph of the coke formed after cracking of Athabasca vacuum residue with 1.0 wt % catalyst under hydrogen at 4.8 MPa and 440 °C stirred at 140 rpm. Sample was heated for 90 min in the hot-stage reactor. (a) Catalyst attaches to the outer surface of mesophase domains. (b) Catalyst can prevent the coalescence of mesophase domains.

has the potential to build higher molecular weight molecules that result in the formation of coke. The condensation of these molecules can result in the formation of aggregates of planar polyaromatic molecules in mechanism a. As a result, the addition of catalyst can suppress the formation or growth of submicrometer mesophase domains. This mechanism can explain the delay in on-set time of observable mesophase in Figure 6 when catalyst is present.

In addition to the expected chemical effect, the dispersed catalyst had an important physical effect by inhibiting the coalescence of the submicrometer domains. Any adhesion of catalyst particles to the exterior of the mesophase domains could hinder coalescence (Figure 10b). Stabilization of the small particles by steric repulsion can explain the smaller area fraction of the larger bulk mesophase domains in the experiments with catalyst. The freeze-fractured surface of the collected coke (coke that remained in the hot-stage after the cracking of vacuum residue under hydrogen) was observed by SEM, as shown in Figure 11. The micrometer-scale mesophase domains are easily detectable in Figure 11a; however, the sample is covered with many submicrometer mesophase domains. This was also consistent with our hypothesis that the first mode of the size distribution contains a large amount of submicrometer scale domains that are not detectable with optical microscopy, and the peak of this mode probably lies at a size below the resolution of an optical microscope. The catalyst particles were detected in the backscattered image (Figure 11b), and the presence of catalyst metal on the surface of the domains was confirmed by EDX analysis. The catalyst particles are again attached to the outer surface of mesophase domains.

The literature on dispersed catalysts emphasizes the nanosize of the particles. In practice, nanosized particles invariably cluster together under reactor conditions.[44] At low catalyst concentrations, the clustering of the catalyst particles is not extensive and the resulting agglomerates are still very small, as can be seen in Figure 10. Due to the limited agglomeration of catalyst particles at low concentration, they were apparently more effective for preventing the growth of larger mesophase domains, that is, preventing 570 μm^2 domains from growing to over 2000 μm^2.

As previously discussed, the initial submicrometer mesophase domains are not detectable by optical microscopy.[45,46] While a nanosized catalyst that is well dispersed in the reactor should be able to prevent submicrometer mesophase domains from further coalescence by steric repulsion, the micrographs

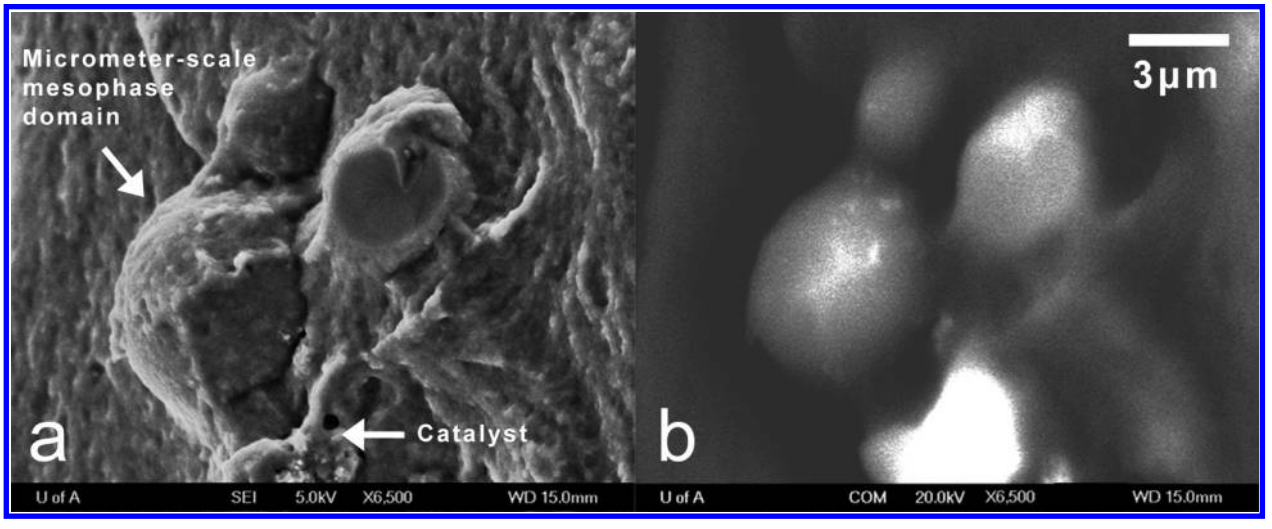

Figure 11. Freeze-fractured surface of coke from Athabasca vacuum residue premixed with 1 wt % of catalyst under SEM. Sample was heated for 90 min in the hot-stage reactor at 440 °C under hydrogen at 4.8 MPa and 440 °C stirred at 140 rpm. (a) Secondary mode image. Some micrometer-scale mesophase spheres are detectable. The surface is also completely covered with submicrometer domains. (b) Backscattered mode image showing the presence of some catalyst particles at the outer surface of mesophase micrometer-scale domains.

dx.doi.org/10.1021/ef300321g | *Energy Fuels* 2012, 26, 3167–3178

indicate small-scale agglomeration of the catalyst at low concentrations. In theory, well-dispersed nanosized catalyst particles could inhibit the coalescence of the submicrometer domains. Agglomeration of catalyst particles, which increases their size and reduces their exterior surface area, makes them less effective at suppressing the coalescence of these submicrometer mesophase domains (Figure 12a). They are,

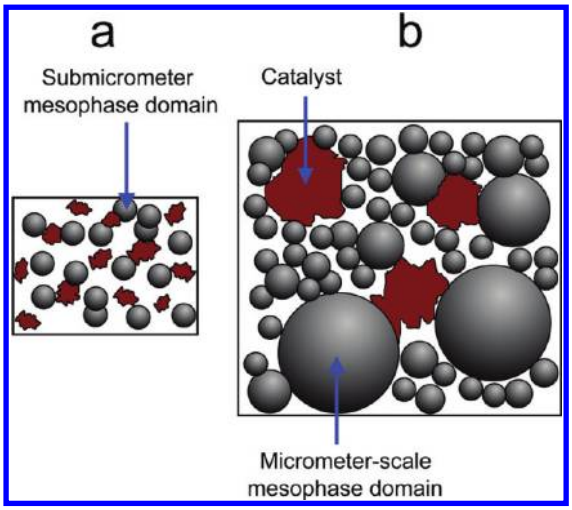

Figure 12. Schematic representation of the interaction of catalyst with mesophase domains. (a) The nano size catalyst prevents the coalescence of submicrometer mesophase domains, but (b) the agglomerated catalyst particles are not effective in suppressing the coalescence of submicrometer mesophase domains anymore; however, they can prevent the coalescence of larger (micrometer-scale) mesophase domains.

however, still effective at stabilizing larger micrometer-scale mesophase domains (Figure 12b). This role is consistent with the data of Figure 6. For small particles with areas below 2000 μm^2, mesophase formation started sooner without catalyst, but the area fraction increased almost at the same rate with and without catalyst. Conversely, for big particles with areas more than 2000 μm^2, the area fraction increased at a significantly lower rate with the addition of catalyst. Mechanisms b and c in Figure 9 would be mainly responsible for the formation mesophase particles with area below 2000 μm^2. These steps would not be affected by catalyst since catalyst could not suppress the coalescence of submicrometer domains and molecular clusters. The catalyst also could not prevent the formation of the bimodal distribution, since it was not effective on mechanisms e and f in Figure 9. However, the catalyst was apparently very effective in suppressing the growth of bulk mesophase by influencing mechanisms d and g and h in Figure 9, since larger domains were involved in these mechanisms and agglomerated catalyst particles can attach to the outer surface of these large domains and suppress their coalescence.

Effect of Catalyst Concentration on Mesophase Formation. The catalyst used in this study was supplied as a fine power. Figure 13 shows the effect of catalyst concentration on the onset of mesophase observation at 4.8 MPa and 450 °C. The results show that the most effective concentration of catalyst, as measured by the maximum time for the onset of mesophase formation, was 1 wt % of catalyst. At higher catalyst loading, the effectiveness of the catalyst decreased significantly.

Very few studies have looked at the effect of the dispersed catalyst concentration on coke yield. Bearden and Aldridge[47]

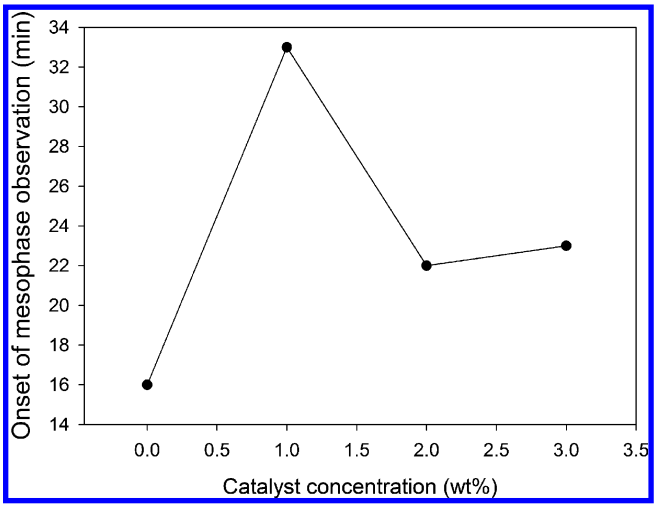

Figure 13. Onset of mesophase observation versus the concentration of catalyst during cracking of Athabasca vacuum residue under hydrogen at 4.8 MPa and 450 °C stirred at 140 rpm.

studied the effect of metal sulphide catalyst on the coke yield. They found that initially the coke yield decreased with molybdenum concentration and reached a minimum when molybdenum concentration was 500−800 ppm. Above that concentration the coke yield slowly increased with increasing the molybdenum concentration. The work of Kennepol and Sanford[15] showed the same effect on coke yield for micro-dispered molybdenum sulphide catalyst, and the work of Panariti et al.[16] showed similar results for dispersed molybdenite. These results suggest that dispersed catalysts at low concentrations are effective in suppressing mesophase and coke formation, but this efficiency decreases at higher concentrations. This effect is not limited to catalyst but can be extended to include other noncatalytic solids. Liu[48] studied the effect of the addition of vacuum residue solids to solid-free vacuum residue on coke yield. A minimum ultimate coke yield was observed at an intermediate concentration of solids. These results suggest that this behavior can be attributed to the physical role of catalyst in suppressing mesophase and coke formation. As we mentioned before, a nanodispersed catalyst has both a chemical and physical role in suppressing the coalescence of submicrometer mesophase domains. In addition, the chemical effect is much more effective with highly dispersed catalyst particles because of the higher surface area. At high concentrations, large scale agglomeration of the catalyst can significantly decrease the efficiency of catalyst in terms of both the physical and chemical effects.

To demonstrate this large-scale agglomeration, the coke that remained in the hot-stage after the cracking of vacuum residue under hydrogen with 3 wt % at 4.8 MPa and 450 °C was collected and observed by SEM, as shown in Figure 14. Rather than the finely distributed catalyst particles and small aggregates that were observed at an initial concentration of 1%, the catalyst particles in this sample were highly agglomerated. Catalyst agglomeration in this case resulted in a decrease in the onset time of observable mesophase formation.

■ CONCLUSIONS

The in situ mesophase formation in Athabasca vacuum residue was investigated using a novel stirred hot-stage reactor. Mesophase formation was studied in vacuum residue under

dx.doi.org/10.1021/ef300321g | Energy Fuels 2012, 26, 3167−3178

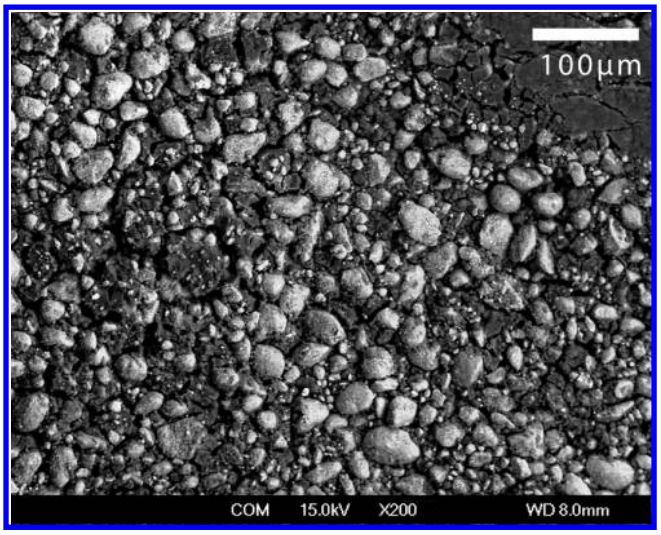

Figure 14. SEM photograph of the coke formed after cracking of Athabasca vacuum residue with 3.0 wt % catalyst under hydrogen at 4.8 MPa and 450 °C stirred at 140 rpm. the sample was heated for 35 min in the hot-stage reactor. Using a higher concentration of catalyst led to significant agglomeration of catalyst particles.

hydrogen atmosphere with and without the addition of catalyst. Stirring forced coalescence, which results in the formation of large bulk mesophase regions in the pitch, which coexisted with a large number of small mesophase domains. Stirring resulted in the formation of a bimodal distribution of mesophase particles in the reacting fluid, resulting in a bimodal distribution comprised of a large number of small spherical mesophase domains and a small number of very large bulk mesophase domains. The addition of catalyst had both chemical and physical effects on mesophase formation. The chemical effect increased the time of onset of mesophase observation, and the physical effect decreased the tendency of mesophase spheres to form bulk mesophase. SEM analysis showed that catalyst particles agglomerated and stuck to the outer surface of mesophase domains and prevented their coalescence. Although the agglomeration of catalyst particles likely decreased its efficiency for suppressing the formation of small mesophase domains of a few micrometers in diameter, the agglomerated material was still effective in suppressing the formation of bulk mesophase. The results showed that there was a maximum for the onset of mesophase observation versus catalyst concentration. As a result, further testing should be undertaken in larger-scale reactors to test if increasing the concentration of catalyst increases the efficiency for suppressing mesophase formation or if instead there is a net reduction in efficiency due to extensive large-scale agglomeration of catalyst particles at high catalyst concentrations.

AUTHOR INFORMATION

Corresponding Author

*Telephone: 780-492-6733. E-mail: william.mccaffrey@ualberta.ca.

Notes

The authors declare no competing financial interest.

ACKNOWLEDGMENTS

The authors would like to acknowledge financial support for this work from UOP LLC.

REFERENCES

(1) Dolbear, G. E. *Petroleum Chemistry and Refining*; Speight, J. G., Ed.; Taylor & Francis: Washington, DC, 1998; Chapter 7.
(2) Speight, J. G. *The Chemistry and Technology of Petroleum*, 4th ed.; CRC Press: Boca Raton, FL, 2006.
(3) Carbonell, M. M.; Guirardello, R. Modelling of a Slurry Bubble Column Reactor Applied to the Hydroconversion of Heavy Oils. *Chem. Eng. Sci.* **1997**, *52*, 4179−4185.
(4) Gray, M. R. *Upgrading Petroleum Residues and Heavy Oils*; Marcel Dekker Inc.: New York, 1994.
(5) Rahmani, S.; McCaffrey, W.; Elliott, J. A. W.; Gray, M. R. Liquid-Phase Behavior during the Cracking of Asphaltenes. *Ind. Eng. Chem. Res.* **2003**, *42* (17), 4101−4108.
(6) Marsh, H.; Latham, C. S. The Chemistry of Mesophase Formation. *Am. Chem. Soc. Symp. Ser.* **1986**, *303*, 1−28.
(7) Brooks, J. D.; Taylor, G. H. Formation of Graphitizing Carbons from Liquid Phase. *Nature* **1965**, *206* (4985), 697−699.
(8) Bisoyi, H. K.; Kumar, S. Discotic Nematic Liquid Crystals: Science and Technology. *Chem. Soc. Rev.* **2010**, *39* (1), 264−285.
(9) Honda, H. Carbonaceous Mesophase-History and Prospects. *Carbon* **1988**, *26* (2), 139−156.
(10) Rahimi, P.; Gentzis, T. The Chemistry of Bitumen and Heavy Oil Processing. In *Practical Advances in Petroleum Processing*; Hsu, C. S., Robinson, P. R., Eds.; Springer: New York, 2006.
(11) Delbianco, A.; Panariti, N.; Dicarlo, S.; Beltrame, P. L.; Carniti, P. New Developments in Deep Hydroconversion of Heavy Oil Residues with Dispersed Catalysts 0.2. Kinetics Aspects of Reaction. *Energy Fuels* **1994**, *8* (3), 593−597.
(12) Pruden, B.; Denis, J. M.; Muir, G. Upgrading of Cold Lake Heavy Oil in the CANMET Hydrocracking Demonstration Plant Process. *4th ITAR/UNDP Conference on Heavy Crude Tar Sands*, Edmonton, 1989.
(13) Miki, Y.; Yamadaya, S.; Oba, M.; Sugimoto, Y. Role of Catalyst in Hydrocracking of Heavy Oil. *J. Catal.* **1983**, *83* (2), 371−383.
(14) Gray, M. R.; Khorasheh, F.; Wanke, S. E.; Achia, U.; Krzywicki, A.; Sanford, E. C.; Sy, O. K. Y.; Ternan, M. Role of Catalyst in Hydrocracking of Residues from Alberta Bitumens. *Energy Fuels* **1992**, *6* (4), 478−485.
(15) Kennepohl, D.; Sanford, E. Conversion of Athabasca Bitumen with Dispersed and Supported Mo-Based Catalysts as a Function of Dispersed Catalyst Concentration. *Energy Fuels* **1996**, *10* (1), 229−234.
(16) Panariti, N.; Del Bianco, A.; Del Piero, G.; Marchionna, M.; Carniti, P. Petroleum Residue Upgrading with Dispersed Catalysts Part 2. Effect of Operating Conditions. *Appl. Catal., A* **2000**, *204* (2), 215−222.
(17) Zhang, S.; Liu, D.; Deng, W.; Que, G. A Review of Slurry-Phase Hydrocracking Heavy Oil Technology. *Energy Fuels* **2007**, *21* (6), 3057−3062.
(18) Dierking, I. *Textures of Liquid Crystals*; Wiley-VCH: Weinheim, 2003.
(19) Lewis, R. T. Hot-Stage Microscopy of Mesophase Pitches. *Ext. Abstr. 12th Bienn. Am. Conf. Carbon, Am. Carbon Soc.* **1975**, 215−216.
(20) Perrotta, A. J.; McCullough, J. P.; Beuther, H. Pressure−Temperature Microscopy of Petroleum-Derived Hydrocarbons. *Prepr. Pap. Am. Chem. Soc., Div. Pet. Chem.* **1983**, *28* (3), 633−639.
(21) Rodriguez, J.; Tierney, J. W.; Wender, I. In Situ Evaluation of the Carbonization Behavior of Graphitizable Carbon Precursors. *Am. Chem. Soc. Div. Fuel Chem.* **1991**, *36*, 1081−1087.
(22) Lafdi, K.; Bonnamy, S.; Oberlin, A. Mechanism of Anisotropy Occurrence in a Pitch Precursor of Carbon-Fibers 0.3. Hot Stage Microscopy of Pitch-B and Pitch-C. *Carbon* **1991**, *29* (7), 857−864.
(23) Rahimi, P.; Gentzis, T.; Dawson, W. H.; Fairbridge, C.; Khulbe, C.; Chung, K.; Nowlan, V.; DelBianco, A. Investigation of Coking Propensity of Narrow Cut Fractions from Athabasca Bitumen Using Hot-Stage Microscopy. *Energy Fuels* **1998**, *12* (5), 1020−1030.
(24) Chwastiak, S.; Lewis, R. T.; Ruggiero, J. D. Quantitative Determination of Mesophase Cnotent in Pitch. *Carbon* **1981**, *19* (5), 357−363.

(25) Moriyama, R.; Hayashi, J.; Suzuki, K.; Hiroshima, T.; Chiba, T. Analysis and Modeling of Mesophase Sphere Generation, Growth and Coalescence upon Heating of a Coal Tar Pitch. *Carbon* **2002**, *40* (1), 53−64.
(26) Braun, M.; Kramer, J.; Huttinger, K. J. Kinetics of Mesophase Formation in a Stirred-Tank Reactor and Properties of the Products 0.6. Catalysis by Iron Benzoate and Naphthoate. *Carbon* **1995**, *33* (10), 1359−1367.
(27) Bernhauer, M.; Braun, M.; Huttinger, K. J. Kinetics of Mesophase Formation in a Stirred-Tank Reactor and Properties of the Products 0.5. Catalysis by Ferrocene. *Carbon* **1994**, *32* (6), 1073−1085.
(28) Bagheri, S. R.; Gray, M. R.; McCaffrey, W. C. Influence of Depressurization and Cooling on the Formation and Development of Mesophase. *Energy Fuels* **2011**, *25* (12), 5541−5548.
(29) Cai, H. Y.; Shaw, J. M.; Chung, K. H. Hydrogen Solubility Measurements in Heavy Oil and Bitumen Cuts. *Fuel* **2001**, *80* (8), 1055−1063.
(30) Callister, W. D.; Rethwisch, D. G. *Fundamentals of Materials Science and Engineering: An Integrated Approach*, 7th ed.; John Wiley & Sons: Hoboken, NJ, 2007.
(31) Fitzer, E.; Kochling, K. H.; Boehm, H. P.; Marsh, H. Recommended Terminology for the Description of Carbon as a Solid (IUPAC Recommendations 1995). *Pure Appl. Chem.* **1995**, *67* (3), 473−506.
(32) Paul, E. L.; Atiemo-Obeng, V. A.; Kresta, S. M. *Handbook of Industrial Mixing: Science and Practice*: Wiley-Interscience: Hoboken, NJ, 2004.
(33) Shields, S. P.; Richards, V. N.; Buhro, W. E. Nucleation Control of Size and Dispersity in Aggregative Nanoparticle Growth. A Study of the Coarsening Kinetics of Thiolate-Capped Gold Nanocrystals. *Chem. Mater.* **2010**, *22* (10), 3212−3225.
(34) Yang, Y.; Corona Iii, A.; Henson, M. A. Experimental Investigation and Population Balance Equation Modeling of Solid Lipid Nanoparticle Aggregation Dynamics. *J. Colloid Interface Sci.* **2012**, *374* (1), 297−307.
(35) Monnoyer, P.; Fonseca, A.; Nagy, J. B. Preparation of Colloidal AgBr Particles from Microemulsions. *Colloids Surf., A* **1995**, *100*, 233−243.
(36) Tojo, C.; Blanco, M. C.; LopezQuintela, M. A. Preparation of Nanoparticles in Microemulsions: A Monte Carlo Study of the Influence of the Synthesis Variables. *Langmuir* **1997**, *13* (17), 4527−4534.
(37) Park, K. S.; Lee, B. W.; Choi, M. An Analysis of Aerosol Dynamics in the Modified Chemical Vapor Deposition. *Aerosol Sci. Technol.* **1999**, *31* (4), 258−274.
(38) Berry, E. X. Cloud Droplet Growth by Collection. *J. Atmos. Sci.* **1967**, *24* (6), 688−701.
(39) Shaw, R. A. Particle−Turbulence Interactions in Atmospheric Clouds. *Annu. Rev. Fluid Mech.* **2003**, *35*, 183−227.
(40) Berry, E. X.; Reinhard, R. L. Analysis of Cloud Drop Growth by Collection: Part 1. Double Distributions. *J. Atmos. Sci.* **1974**, *31* (7), 1814−1824.
(41) Marsh, H.; M.A., D. Mesophase of Graphitizable Carbons. In *Liquid Crystalline and Mesomorphous Polynzers*; Shibaev, V. P., Lam, L., Eds.; Springer: New York, 1993; pp 231−257.
(42) Marsh, H.; Martinez-Escandell, M.; Rodriguez-Reinoso, F. Semicokes from Pitch Pyrolysis: Mechanisms and Kinetics. *Carbon* **1999**, *37* (3), 363−390.
(43) Gray, M. R.; McCaffrey, W. C. Role of Chain Reactions and Olefin Formation in Cracking, Hydroconversion, and Coking of Petroleum and Bitumen Fractions. *Energy Fuels* **2002**, *16* (3), 756−766.
(44) Chianelli, R. R.; Siadati, M. H.; De la Rosa, M. P.; Berhault, G.; Wilcoxon, J. P.; Bearden, R.; Abrams, B. L. Catalytic Properties of Single Layers of Transition Metal Sulfide Catalytic Materials. *Catal. Rev.: Sci. Eng.* **2006**, *48* (1), 1−41.
(45) Oberlin, A. High Resolution TEM Studies of Carbonization and Graphitization. In *Chemistry and Physics of Carbon*; Marcel Dekker: New York, 1989; Vol. *22*, pp 1−143.
(46) Qian, Z.; Clarke, D. E.; Marsh, H. Structure in Cokes from Coals of Different Rank. *Fuel* **1983**, *62* (9), 1084−1089.
(47) Bearden, R.; Aldridge, C. L. Novel Catalyst and Process to Upgrade Heavy Oil. *Energy Prog.* **1981**, *1*, 1−4.
(48) Liu, L. Effect of Solids on Coke Formation from Athabasca Bitumen and Vacuum Residue. Ph.D. Thesis, University of Alberta, Edmonton, 2002.